# Plasma heating and asymmetric reconnection in CMEs

Nick Murphy

Harvard-Smithsonian Center for Astrophysics

September 28, 2010

Collaborators: John Raymond, Kelly Korreck, Carl Sovinec, Paul Cassak, Jun Lin, Chengcai Shen, & Aleida Young

# Outline

- Plasma heating rates of the 28 June 2000 CME
  - Observations (UVCS, LASCO, EIT, MLSO/MK4, *GOES*)
  - Using a time-dependent ionization analysis to constrain heating
  - Candidate mechanisms and connections with the laboratory
- Asymmetric reconnection in CME current sheets
  - A scaling analysis of asymmetric outflow reconnection
  - Simulations of X-line retreat
  - Deriving an expression for X-line motion

# Introduction

- The understanding of astrophysical phenomena usually begins with the energy budget
- The kinetic and potential energies of CMEs can be obtained using white light coronagraph measurements (e.g., Vourlidas *et al.* 2000)
- The magnetic field of the corona is difficult to diagnose
- The Ultraviolet Coronagraph Spectrometer (UVCS) on *SOHO* allows us to study the thermal energy content of CMEs
- We consider the physics behind one heating mechanism in detail: upflow from the CME current sheet

# On 28 June 2000, a fast and powerful CME was observed by *SOHO*/UVCS

- *SOHO*/EIT 195 Å observations show a rising dark arcade between 18:00–18:48
- *GOES* observed a C3.7 class X-ray flare starting at 18:48 UT
- While light coronagraph observations by the Mauna Loa Solar Observatory (MLSO) show possible kinking of the rising flux rope
- Ciaravella *et al.* (2005) use UVCS and LASCO measurements to detect a coronal shock wave driven by this event
- A fast, powerful CME with a weak flare

# *SOHO*/EIT observations show a rising dark arcade at 195 Å followed by bright He II arches at 304 Å

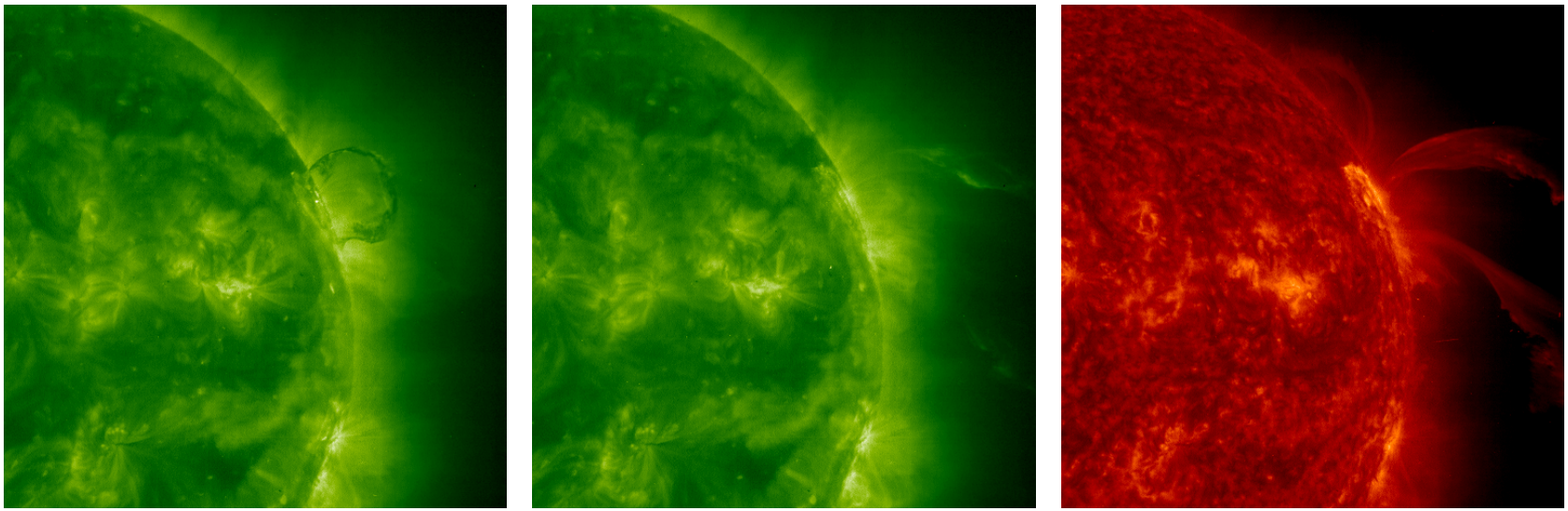

- *From left to right:* 195 Å at 18:48 UT and 19:13 UT, and 304 Å at 19:19 UT

# *SOHO*/LASCO observations show the rising prominence crossing the UVCS slit

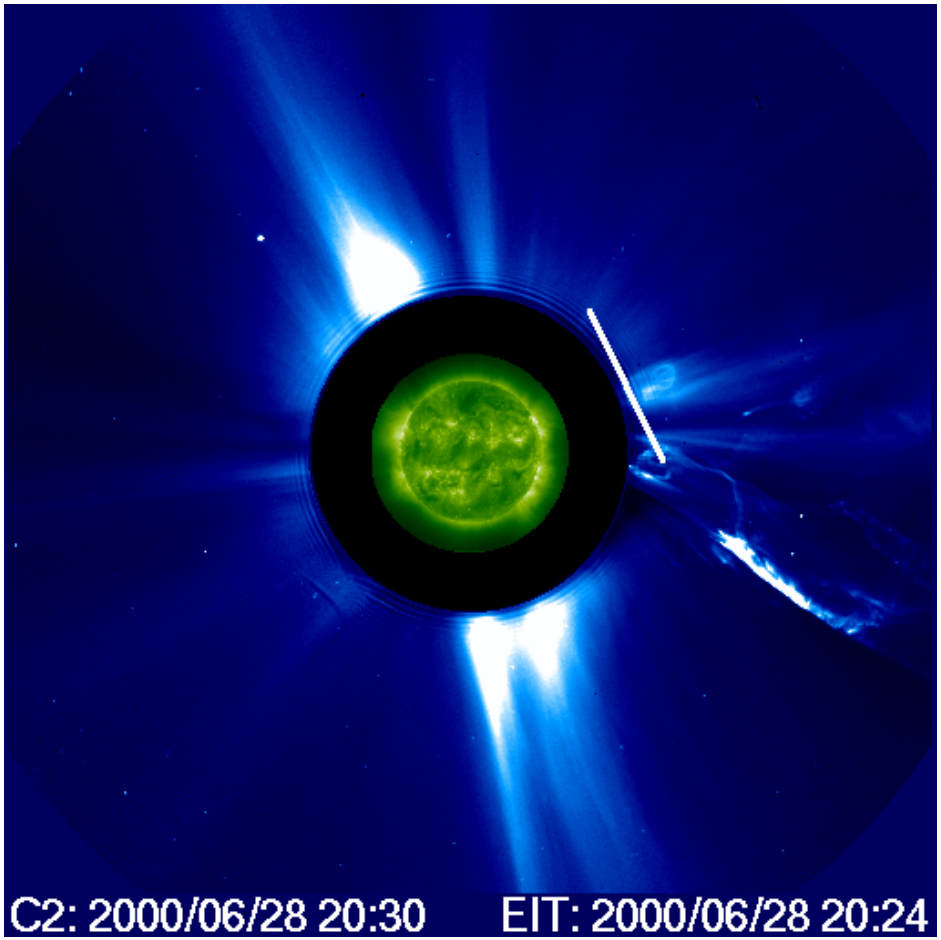

# We use two independent methods to find UVCS densities

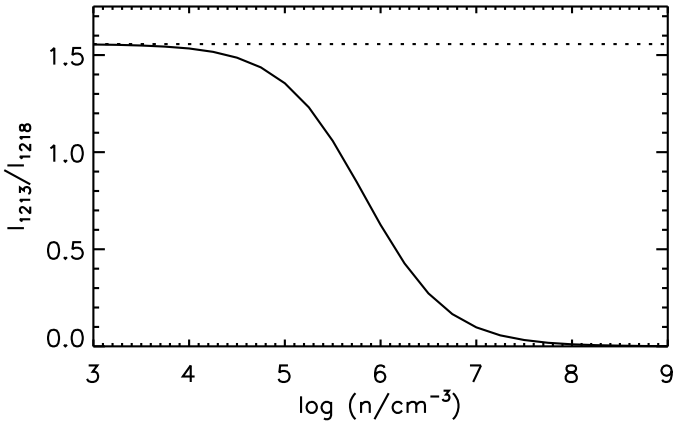


1. The ratio of the [O V] $\lambda$1213.9 forbidden line to the O V] $\lambda$1218.4 intercombination line (Akmal *et al.* 2001)
2. Radiative pumping of the O VI $\lambda\lambda$1031.9, 1037.61 doublet by chromospheric Ly $\beta$, O VI, or C II emission (Raymond & Ciaravella 2004, Noci *et al.* 1987)
   - The collisional ratio is 2:1, so departures from this are due to radiative pumping
   - Provides both density and total velocity information

# From LASCO and UVCS observations we identify six features to analyze

| Blob | Time | $\log n_e$ | Description |
|---|---|---|---|
| A | 19:12 | 7.0 | Near leading edge |
| B | 19:14 | 7.2 | Near leading edge |
| C | 19:16 | 6.7 | Between leading edge and prominence |
| D | 19:21 | 6.6 | Between leading edge and prominence |
| E | 19:27 | 6.6 | Between leading edge and prominence |
| F | 20:11 | 6.6 | Prominence |

# UVCS observations show a diagonal feature in O V and O VI at 20:11 UT (Blob F)

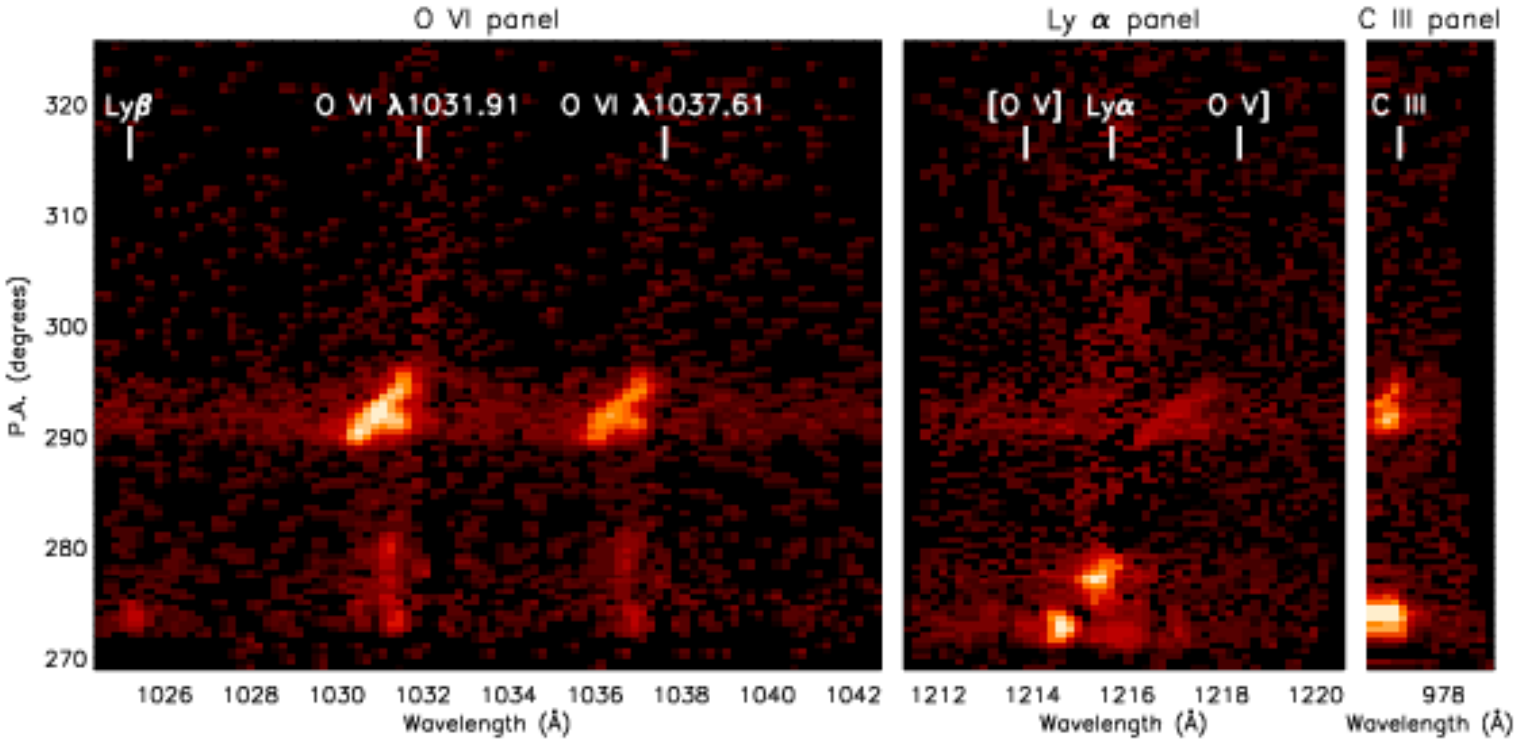


- Observed lines include O V, O VI, Ly$\alpha$, Ly $\beta$, C II, C III, N III

# Weak Ly$\alpha$ in Blob F allows both [O v] and O v] to be observed

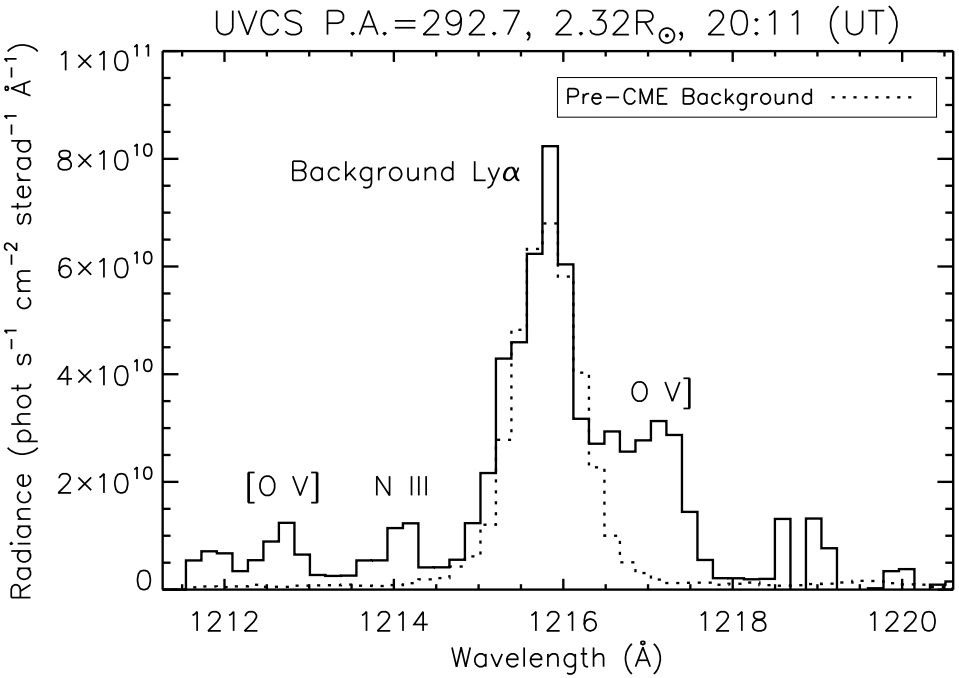


- The N III $\lambda\lambda 989, 991$ lines sometimes appear at the same position on the detector as [O v] at 1213.9 Å

# We use a 1-D time-dependent ionization code to track ejecta between the flare site and UVCS slit

- We run a grid of models with different initial densities, initial temperatures, and heating rates (e.g, Akmal *et al.* 2001)
- The final density is derived from UVCS observations
- Assume homologous expansion
- Multiple heating parameterizations
  - An exponential wave heating model by Allen *et al.* (1998)
  - The expanding flux rope model by Kumar & Rust (1996)
  - Heating proportional to $n$ or $n^2$
- Velocities are scaled from Maričić *et al.* (2006)
- The models consistent with UVCS observations give the allowable range of heating rates

# Caveats and considerations

- Observations are averaged across the line of sight
  - UVCS may be observing multiple components at different temperatures simultaneously
  - We assume that O V and O VI emission is from the same plasma, and take Ly$\alpha$, C II, C III, and N III emission as upper limits
- Some heating parameterizations are not amenable to a 1-D analysis
  - Reconnection outflow from the CME current sheet
  - Kink-like motions driving waves which then dissipate
- No physical heating mechanism is assumed, except for the wave heating model

# Total heating, kinetic energy, and potential energy (keV/proton)

| Blob | $Q_{\rm AAH}$ | $Q \propto n$ | $Q \propto n^2$ | $Q_{\rm KR}$ | K.E. | P.E. |
|---|---|---|---|---|---|---|
| A | 1.0–3.8 | 2.3–9.0 | — | 1.1–29 | 28 (>6.0) | 0.78 |
| B | 0.03–3.7 | 2.3–15 | 186-466 | 1.7–44 | 34 (>5.5) | 0.82 |
| C | 0.03–4.0 | 0.1–15 | 30–476 | 0.5–44 | 28 (>5.6) | 0.81 |
| D | 0.02–2.9 | 0.06–11 | 32–511 | 0.8–48 | 28 (>4.0) | 0.83 |
| E | 1.4 | 2.9 | 545 | 2.1–4.7 | 34 (>2.3) | 0.86 |
| F | 1.8–4.4 | 3.1 | — | 12 | 1.4 (>1.1) | 0.57 |

- Lower limits to the kinetic energy are given in parentheses
- Total velocities are estimated using O VI pumping
- $Q \propto n^2$ provides systematically higher heating rates

# Discussion

- The total heating is greater than the kinetic energy in the best constrained feature (Blob F), which is associated with the rising prominence
- C III $\lambda$977 is blueshifted off of the UVCS panel for Blobs A–D but provides a useful constraint when observed
- Radiative pumping of Blob E may be due to chromospheric O I $\lambda\lambda 1027.4, 1028.2$ instead of Ly $\beta$
- The results of this and previous analyses suggest that CME models should take plasma heating into account

# Candidate heating mechanisms include:

- Reconnection outflow from the CME current sheet
  - Recent theoretical/numerical results suggest that most of the energy goes up
- Wave heating from photospheric motions
  - Landi *et al.* (2010) show that heating $\sim$1500 times that of coronal holes would be needed for the 'Cartwheel CME'
- The kink instability of the expanding flux rope
  - But, $V_{\rm kink} < V_{\rm CME}$
- Magnetic dissipation/the tearing instability
- Thermal conduction/energetic particles from flare
  - Unlikely because a C class flare is associated with this event

# Connections with laboratory plasma experiments

- Tripathi and Gekelman (2010) model an erupting flux rope and find that intense magnetosonic waves heat the ambient plasma
- Asymmetric outflow reconnection occurs in spheromak merging experiments (MRX, SSX, TS-3/4)
- Flux rope experiments are performed at MRX, RSX, LAPD, the Caltech spheromak experiment, and elsewhere

# Flux Rope Model of Coronal Mass Ejections

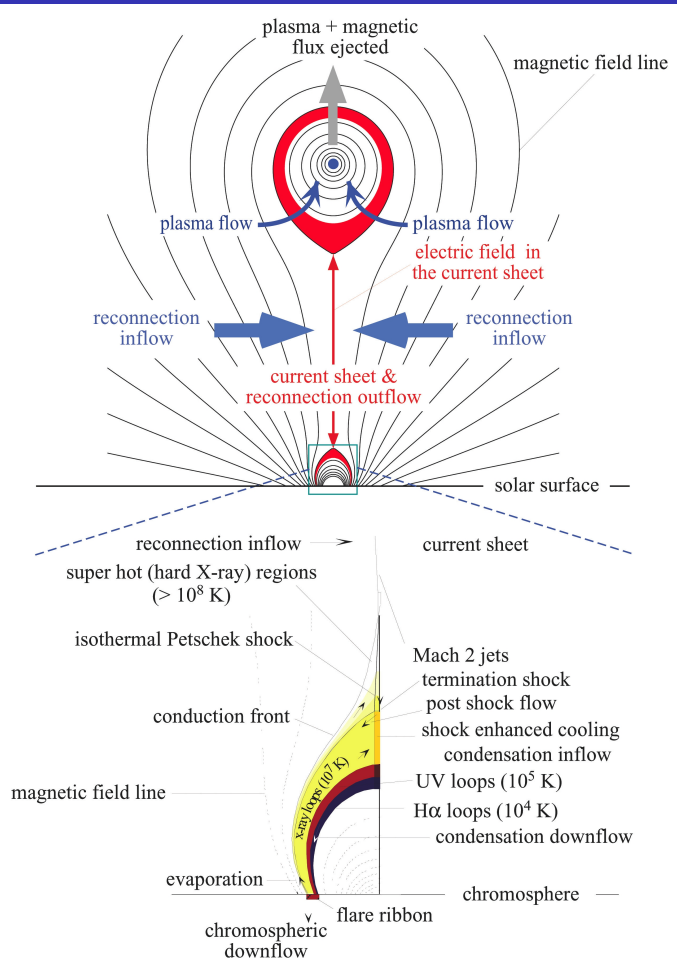


- Many models of CMEs predict a current sheet behind the rising flux rope (e.g., Lin & Forbes 2000)

# Observations of CME current sheets

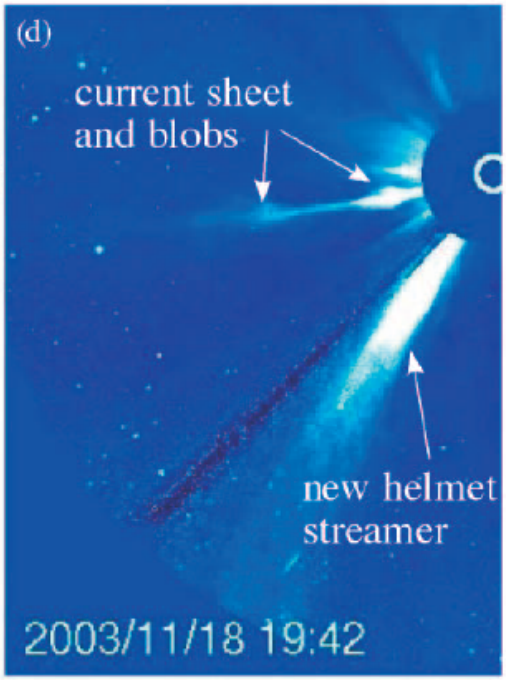


- Current sheets behind CMEs have been observed for a number of events (e.g., Ko *et al.* 2003; Lin *et al.* 2005; Ciaravella & Raymond 2008; Savage *et al.* 2010)
- Outward-moving blobs could be the result of the tearing instability in the current sheet (e.g., Lin *et al.* 2007)

# Is reconnection in CME current sheets symmetric?

- Sunward outflow impacts a region of high plasma and magnetic pressure
- Antisunward outflow encounters the rising flux rope
- The upstream magnetic field strength and density are both strong functions of height
- Seaton (2008) predicts that the majority of the outflow is directed upward towards the rising flux rope, and that the flow stagnation point and magnetic field null should be near the base of the current sheet
- Savage *et al.* (2010) track upflowing (downflowing) features above (below) $h \sim 0.25 R_\odot$ in the 9 April 2008 'Cartwheel' CME current sheet. This is near the X-line in pre-event magnetic field models.

# Developing a model for asymmetric reconnection

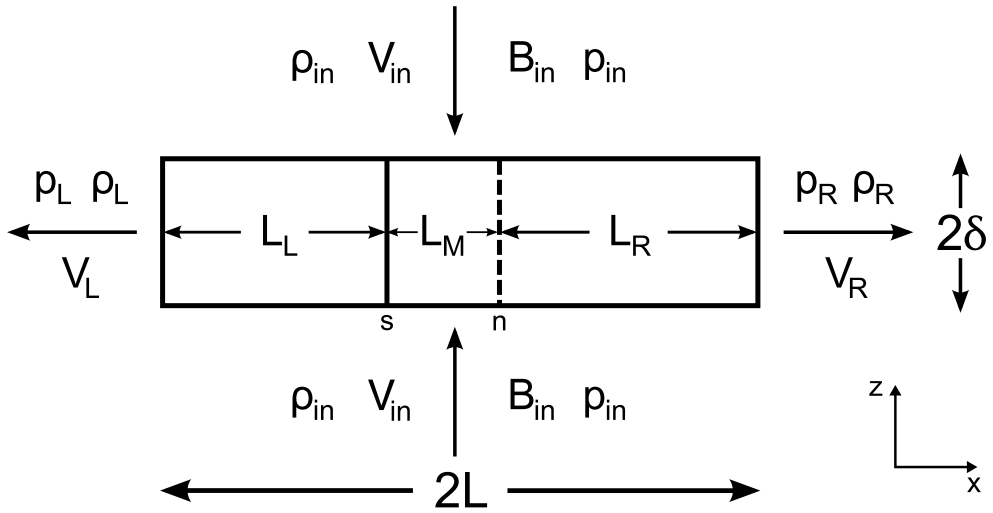


- The above figure represents a long and thin reconnection layer with asymmetric downstream pressure (Murphy, Cassak, & Sovinec, JGR, 2010). Reconnection is assumed to be steady in an inertial reference frame.
- 'n' denotes the magnetic field null and 's' denotes the flow stagnation point

# Finding scaling relations for asymmetric outflow

- From conservation of mass, momentum, and energy we arrive at

$$
\begin{aligned}
2\rho_{in} V_{in} L &\sim \rho_L V_L \delta + \rho_R V_R \delta \\
\rho_L V_L^2 + p_L &\sim \rho_R V_R^2 + p_R \\
2 V_{in} L \left( \alpha p_{in} + \frac{B_{in}^2}{\mu_0} \right) &\sim V_L \delta \left( \alpha p_L + \frac{\rho_L V_L^2}{2} \right) \\
&\quad + V_R \delta \left( \alpha p_R + \frac{\rho_R V_R^2}{2} \right)
\end{aligned}
$$

where $\alpha \equiv \gamma/(\gamma - 1)$ and we ignore upstream kinetic energy/downstream kinetic energy and assume the contribution from tension along the boundary is small or even.

# Deriving the outflow velocity and reconnection rate

- In the incompressible limit

$$V_{L,R}^2 \sim \sqrt{4\left(c_{in}^2 - \frac{\bar{p}}{\rho}\right)^2 + \left(\frac{\Delta p}{2\rho}\right)^2} \pm \frac{\Delta p}{2\rho}$$

  using $\bar{p} \equiv \frac{p_L + p_R}{2}$, $\Delta p \equiv p_R - p_L$, and $c_{in}^2 = \frac{B_{in}^2}{\mu_0 \rho_{in}} + \frac{\alpha p_{in}}{\rho_{in}}$

- By assuming resistive dissipation, the electric field is then given by

$$E_y \sim B_{in}\sqrt{\frac{\eta\left(V_L + V_R\right)}{2\mu_0 L}}$$

# Implications

- The scaling relations show that the reconnection rate is weakly sensitive to asymmetric downstream pressure
  - If one outflow jet is blocked, reconnection will be almost as fast
  - Reconnection will slow down greatly only if both outflow jets are blocked
  - The current sheet responds to asymmetric downstream pressure by changing its thickness or length
- However, this analysis makes three major assumptions:
  - The current sheet is stationary
  - The current sheet thickness is uniform
  - Magnetic tension contributes symmetrically along the boundaries
- To make further progress, we must do numerical simulations

# Resistive MHD simulations of X-line retreat

- The 2-D simulations start from a periodic Harris sheet which is perturbed at two nearby locations ($x = \pm 1$)
- The reconnection layers move away from each other as they develop (Murphy 2010; see also Oka *et al.* 2008)
- Domain: $-30 \leq x \leq 30$, $-12 \leq z \leq 12$
- Simulation parameters: $\eta = 10^{-3}$, $\beta_\infty = 1$, $\mathrm{S} = 10^3$–$10^4$, $\mathrm{Pm} = 1$, $\gamma = 5/3$, $\delta_0 = 0.1$
- Define:
  - $x_n$ is the position of the X-line
  - $x_s$ is the position of the flow stagnation point
  - $V_x(x_n)$ is the velocity *at* the X-line
  - $\frac{\mathrm{d}x_n}{\mathrm{d}t}$ is the velocity *of* the X-line

# NIMROD solves the equations of extended MHD using a finite element formulation (Sovinec *et al.* 2004)

- In dimensionless form, the equations used for these simulations are

$$\frac{\partial \mathbf{B}}{\partial t} = -\nabla \times (\eta \mathbf{J} - \mathbf{V} \times \mathbf{B}) + \kappa_{divb} \nabla \nabla \cdot \mathbf{B} \quad (1)$$

$$\mathbf{J} = \nabla \times \mathbf{B} \quad (2)$$

$$\nabla \cdot \mathbf{B} = 0 \quad (3)$$

$$\rho \left( \frac{\partial \mathbf{V}}{\partial t} + \mathbf{V} \cdot \nabla \mathbf{V} \right) = \mathbf{J} \times \mathbf{B} - \nabla p - \nabla \cdot \rho \nu \nabla \mathbf{V} \quad (4)$$

$$\frac{\partial \rho}{\partial t} + \nabla \cdot (\rho \mathbf{V}) = \nabla \cdot D \nabla \rho \quad (5)$$

$$\frac{\rho}{\gamma - 1} \left( \frac{\partial T}{\partial t} + \mathbf{V} \cdot \nabla T \right) = -\frac{p}{2} \nabla \cdot \mathbf{V} - \nabla \cdot \mathbf{q} + Q \quad (6)$$

# The current sheets have characteristic single wedge shapes

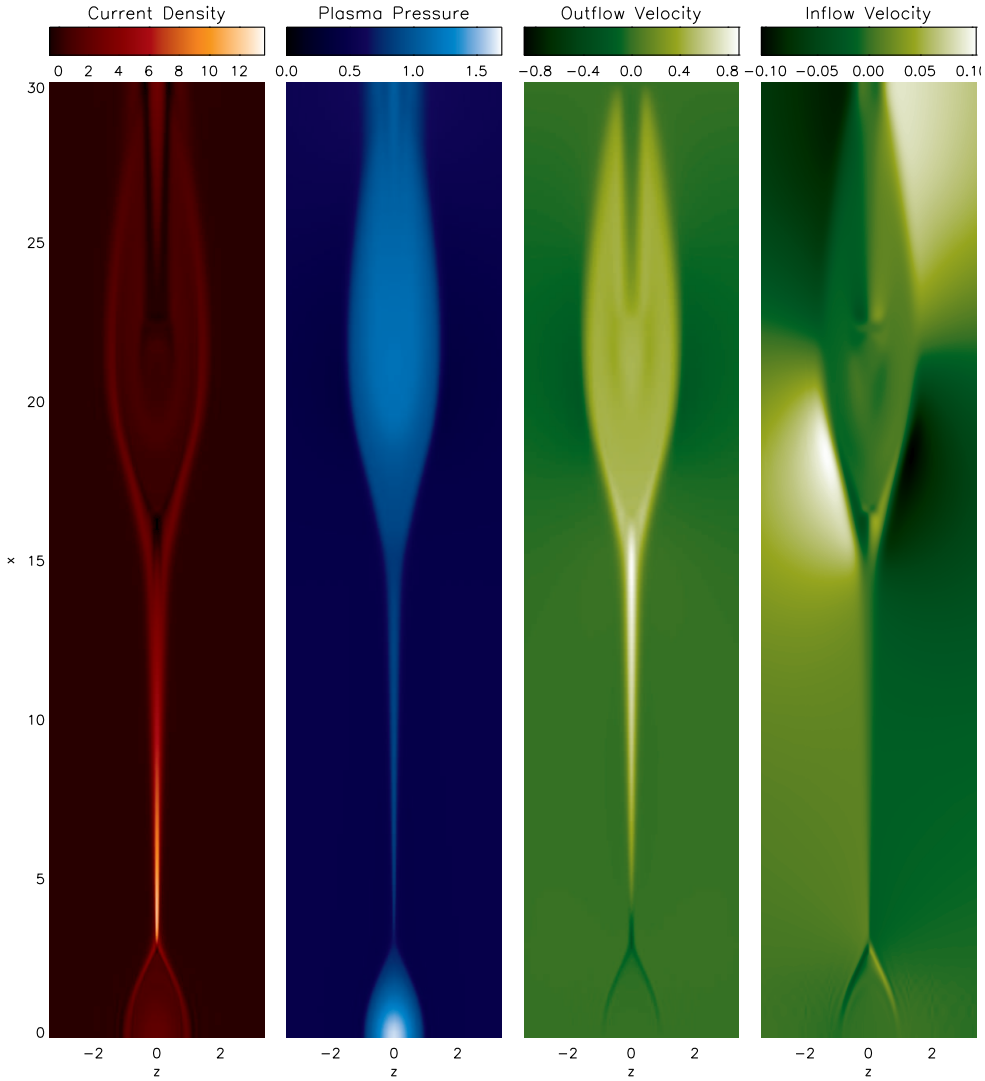

# The outflow away from the obstruction is much faster

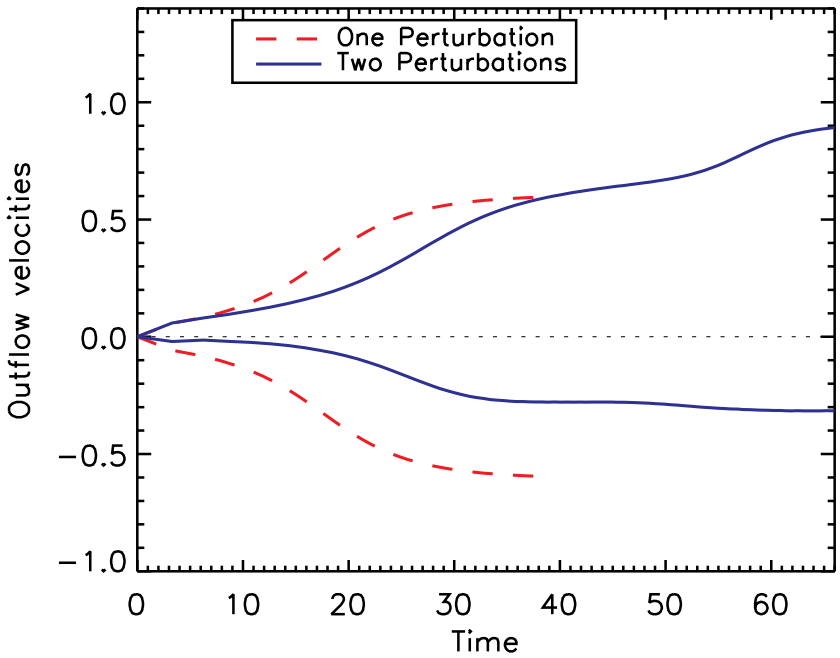


- In agreement with Seaton (2008) and Reeves *et al.* (2010), most of the energy goes away from the obstructed exit

# The flow stagnation point and X-line are not colocated

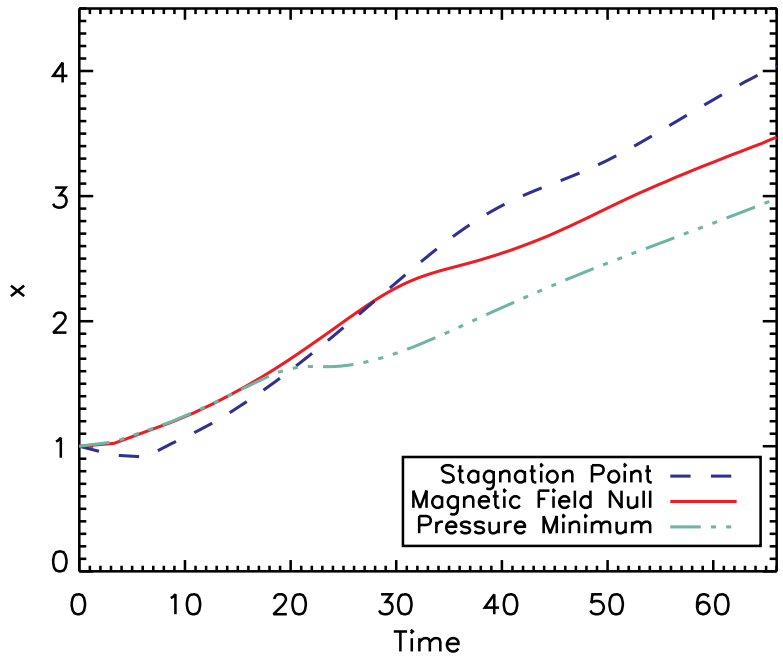


- Surprisingly, the relative positions of the X-line and flow stagnation point switch
- This occurs so that the stagnation point will be located near where the tension and pressure forces cancel

# Late in time, the X-line diffuses against strong plasma flow

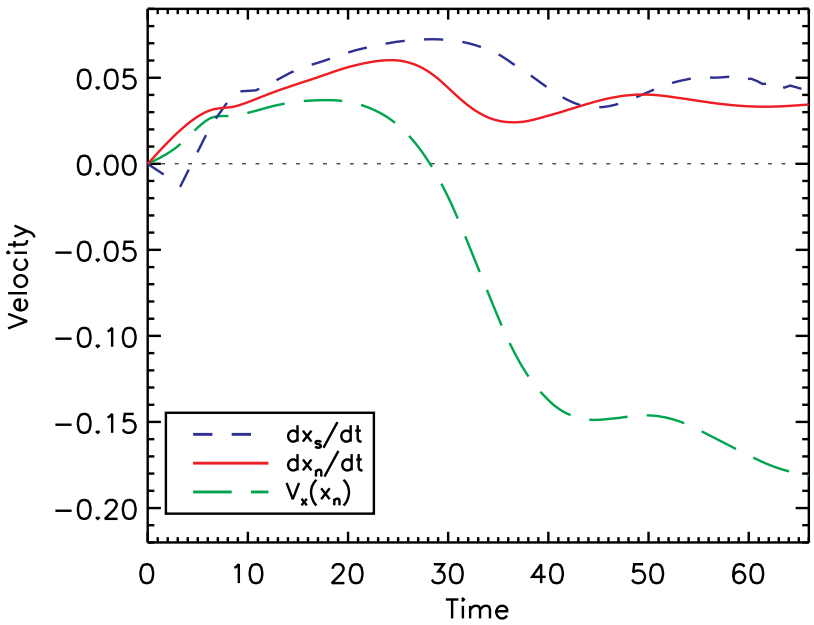


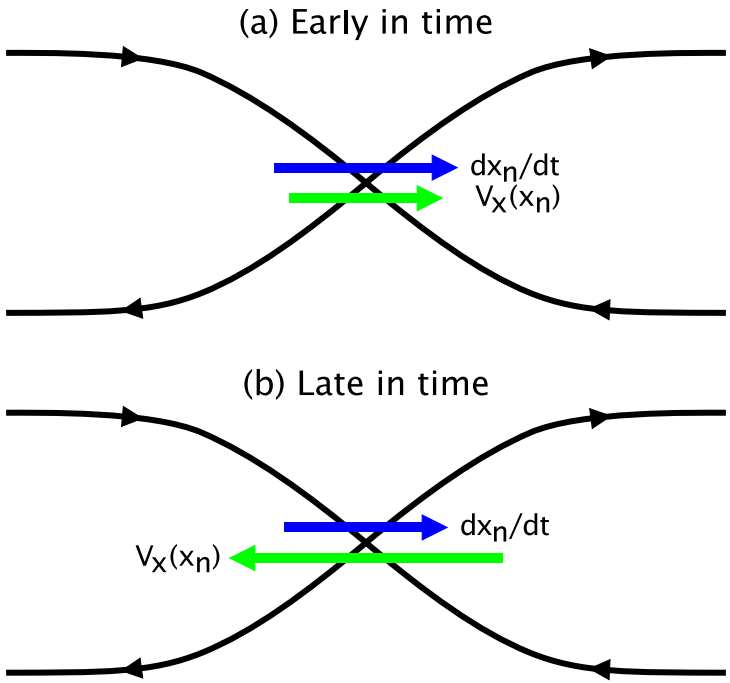


- The stagnation point retreats more quickly than the X-line
- Any difference between $\frac{\mathrm{d}x_n}{\mathrm{d}t}$ and $V_x(x_n)$ is due to diffusion
- The velocity *at* the X-line is not the velocity *of* the X-line

# Deriving an expression for X-line retreat

- The inflow ($z$) component of Faraday's law for the 2D symmetric inflow case is

$$\frac{\partial B_z}{\partial t} = -\frac{\partial E_y}{\partial x} \tag{7}$$

- The convective derivative of $B_z$ at the X-line taken at the velocity of X-line retreat, $\mathrm{d}x_n/\mathrm{d}t$, is

$$\left.\frac{\partial B_z}{\partial t}\right|_{x_n} + \frac{\mathrm{d}x_n}{\mathrm{d}t}\left.\frac{\partial B_z}{\partial x}\right|_{x_n} = 0 \tag{8}$$

# Deriving an expression for X-line retreat

- From Eqs. 7 and 8:

$$\frac{\mathrm{d}x_n}{\mathrm{d}t} = \left.\frac{\partial E_y/\partial x}{\partial B_z/\partial x}\right|_{x_n} \tag{9}$$

- Using $\mathbf{E} + \mathbf{V} \times \mathbf{B} = \eta \mathbf{J}$, we arrive at

$$\frac{\mathrm{d}x_n}{\mathrm{d}t} = V_x(x_n) - \eta \left[\frac{\frac{\partial^2 B_z}{\partial x^2} + \frac{\partial^2 B_z}{\partial z^2}}{\frac{\partial B_z}{\partial x}}\right]_{x_n} \tag{10}$$

- In resistive MHD, usually $\frac{\partial^2 B_z}{\partial z^2} \gg \frac{\partial^2 B_z}{\partial x^2}$
  - This corresponds to diffusion of the normal component of the magnetic field along the inflow direction

# Mechanism and implications

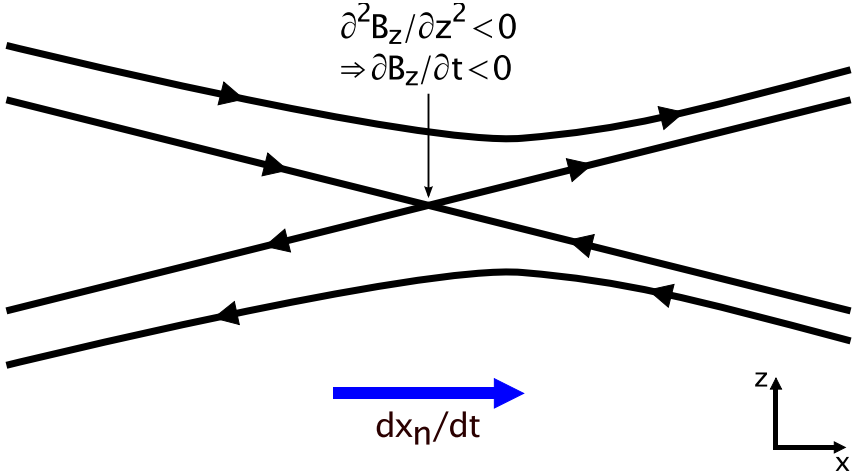


- The X-line moves in the direction of increasing reconnection electric field strength
- X-line retreat occurs through a combination of advection by bulk plasma flow and diffusion of the normal component of the magnetic field
- X-line motion depends intrinsically on local parameters evaluated at the X-line

# Simulations of multiple X-line reconnection

- NIMROD simulations with multiple initial perturbations were analyzed by A. Young
  - Isolated or strong perturbations are more likely to survive
  - Winning X-lines early on have plasma pressure facilitating outflow rather than impeding it
  - When an X-line is located near one end of the current sheet, the flow stagnation point is located in between the X-line and a central plasma pressure maximum
  - The number of X-lines changes due to diffusion of the normal component of the magnetic field
- SHASTA simulations by C. C. Shen and J. Lin show that the direction of plasmoid ejection is related to the relative locations of the flow stagnation point and X-line
  - If $x_s > x_n$, then $V_{\mathrm{plasmoid}} > 0$

# Conclusions

- CME heating occurs even after the ejecta leaves the flare site
- The total heating is comparable to or greater than the kinetic energy of the ejecta
  - Models of CMEs should evolve the energy equation
- Several candidate mechanisms can be ruled out for the 28 June 2000 CME because there is insufficient energy in the flare to heat the ejecta
  - Thermal conduction, energetic particles from flare region
- Asymmetric reconnection in CME current sheets probably causes most of the energy and mass to go upward
- X-line retreat occurs due to a combination of advection by the bulk plasma flow and diffusion of $B_z$

# Open questions

- What mechanism(s) are responsible for heating of CMEs?
- Do flareless CMEs show less heating than CMEs with powerful flares?
- Do fast CMEs show more heating than slow CMEs?
- What is the role of the CME current sheet in the mass and energy budget of CMEs?
- Where are the X-line and flow stagnation line located in CME current sheets?
- What are the roles of the plasmoid and tearing instabilities in CME current sheets?

# Future work

- To answer the questions on the previous slide, we need to investigate multiple events using a standardized method of analysis
  - Therefore, we will perform our time-dependent heating analysis for ∼10–20 CMEs
  - This will allow us to investigate how heating depends on location, CME properties, and other parameters
- We will extend simulations of X-line retreat to include 3-D/two-fluid effects
  - Applicable to the magnetospheric and turbulent reconnection